A novel method for localization of the maximum glenoid bone defect during reverse shoulder arthroplasty

Graeme T. Harding, MASc, MD, FRCSC[a,*], Aaron J. Bois, MD, MSc, FRCSC[b,c], Martin J. Bouliane, MD, FRCSC[a]

[a]Division of Orthopaedic Surgery, University of Alberta, Edmonton, Alberta, Canada
[b]Section of Orthopaedic Surgery, Cumming School of Medicine, University of Calgary, Calgary, Alberta, Canada
[c]McCaig Institute for Bone and Joint Health, University of Calgary, Calgary, Alberta, Canada

Background: Management of glenoid bone defects during reverse shoulder arthroplasty remains a challenge. The aim of our study was to preoperatively localize the maximal depth of glenoid bone defects in relation to glenoid reaming.

Methods: Thirty preoperative shoulder computed tomography scans were collected. Three assessors created standardized surgical plans, using 3-dimensional (3D) computed tomography—based Blueprint planning software in which the reaming axis was held constant at zero degrees of version and inclination. Each plan resulted in a 2-dimensional (2D) image of the reamer's contact on the glenoid and a corresponding 3D representation of the glenoid bone defect. The position of the maximum glenoid defect was localized on both the 2D and 3D images. Descriptive statistics were calculated. The correlation between angles from 2D and 3D images was assessed, and intraclass correlation was used to assess interrater and intrarater reliability.

Results: Twenty-eight patients were included. The overall mean difference between 2D and 3D angles was 5.4° (standard deviation 5.2°). The correlation between 2D and 3D angles was almost perfect. Intraclass correlation results demonstrated near-perfect agreement. The maximal glenoid defect was within 5% of a circle (or +/- 9°) from perpendicular to the high-side ream line in 85.1% of comparisons and was within 10% of a circle in 97.6% of comparisons.

Conclusion: Using Blueprint planning software, we have demonstrated with almost perfect agreement among 3 assessors that when the reaming axis is held constant, the maximum glenoid bone defect is reliably located perpendicular to the glenoid ream line.

The management of severe glenoid bone defects presents a significant challenge in reverse shoulder arthroplasty (RSA).[15] Glenoid bone loss is associated with risks of inaccurate baseplate positioning, prosthetic instability or dislocation, scapular notching, and early implant failure.[20] Given these risks, glenoid bone loss requires appropriate recognition and management. Bone grafting is a well-established method for the management of complex glenoid bone defects.[1,4,13] Advantages of glenoid bone grafting include its restoration of bone within the glenoid vault, normalization of glenoid morphology, and good clinical outcomes.[1,3,4,12,20] As shown in a recent meta-analysis by Paul et al,[16] glenoid bone grafting also demonstrates a high graft union rate, particularly when autograft bone is used.

Given that the indications for reverse shoulder arthroplasty have expanded,[5] the need to manage glenoid bone defects has become relatively common. As many as 15% of primary shoulder arthroplasties require bone grafting, and in the setting of cuff tear arthropathy, this increases to as many as 40%.[12] Tornier Blueprint is an industry-leading 3-dimensional (3D) computed tomography (CT)—based planning software for shoulder arthroplasty, which is now widely available. By using Blueprint for RSA, surgeons can create a preoperative plan including the dimensions of a patient-specific bone graft for restoration of glenoid anatomy in cases of severe deformity. There is wide variability in both the etiology and morphology of glenoid bone defects,[9,12] and this variability contributes to the complexity of intraoperative glenoid bone graft preparation. To simplify intraoperative glenoid bone graft preparation, an initial step is to determine the precise location of the deepest (or maximum) aspect of the glenoid bone defect.
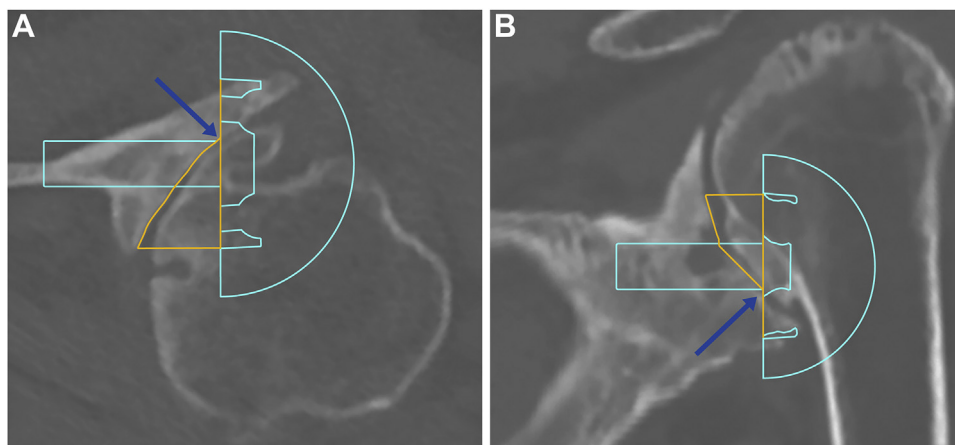
Figure 1 Glenoid baseplate positioning during preoperative planning with Blueprint. (**A**) Axial CT image demonstrates the position of the planned glenoid component in a patient with substantial glenoid retroversion. (**B**) Coronal CT image (different patient) reveals the position of the planned glenoid component in a patient with substantial glenoid inclination. The ⬊ in parts **A** and **B** show that the glenoid is reamed to the post. The patient-specific bone graft is depicted in orange. *CT*, computed tomography.
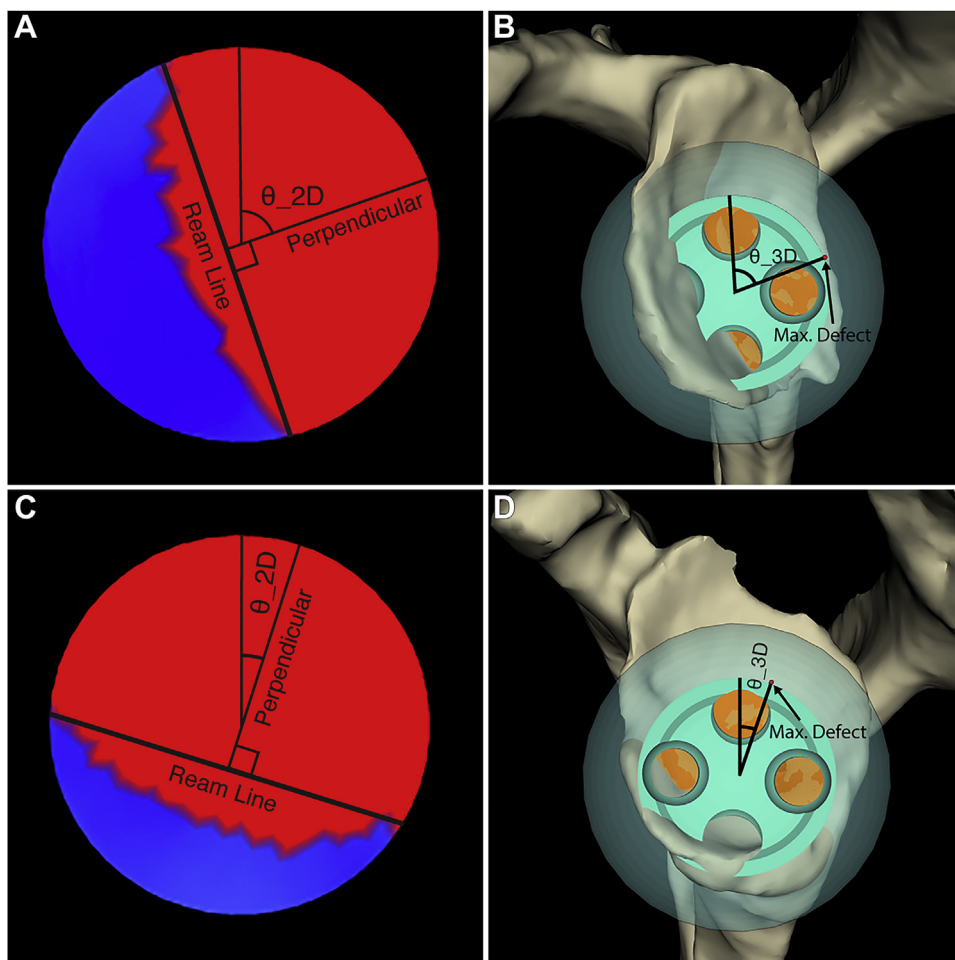
Figure 2 Representative 2D and 3D images for angle measurements. (**A** and **C**) The area of contact between the glenoid reamer and the glenoid fossa (depicted in blue). The estimated line-of-best-fit across the reamed area is also shown (i.e., ream line). Θ_2D represents the angle to a point perpendicular to the ream line. (**B** and **D**) Corresponding 3D "en face" views of the glenoid component, the underlying bone graft in orange, the maximum defect digital marker (⬊), and the angle Θ_3D. *2D*, 2-dimensional; *3D*, 3-dimensional.
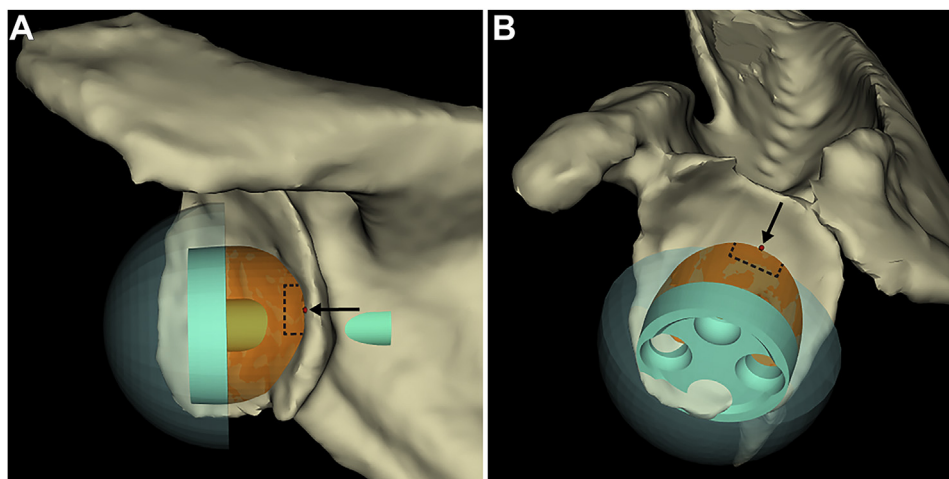
Figure 3 (**A**) Posterior view and (**B**) superior oblique view of the maximum glenoid bone defects with the maximum defect digitial marker shown in red. The ↘ points to the location of the maximum defect.

Table I
Glenoid morphology of N = 28 included patients.

Diagnosis	N	Classification	Morphology
Osteoarthritis	18	Walch B/C	Mean retroversion = 27°
Cuff tear arthropathy	10	Favard E1-E3	Mean inclination = 14°

The purpose of our study was to localize the maximum depth of a variety of glenoid bone defects in relation to glenoid reaming when the reaming axis is held constant. We hypothesized that the maximum glenoid defect would be located perpendicular to a line-of-best-fit created by the high side of the glenoid ream.

Methods

Institutional research ethics board of approval was obtained. Thirty preoperative shoulder CT scans of adult patients who underwent primary reverse shoulder arthroplasty were collected retrospectively from two academic institutions. To be included in the study, a minimum glenoid deformity of 10 degrees in any plane (ie, horizontal and/or vertical plane) was required. Three assessors − 2 fellowship-trained shoulder surgeons and a shoulder fellow (G.T.H.) − created standardized surgical plans for RSA using Tornier Blueprint. A specific preoperative planning sequence was followed for each CT scan. After each CT scan was uploaded into Blueprint, the glenoid was oriented "en face." For simplicity, a reverse shoulder arthroplasty using the Reversed II system was selected for all cases. Standard anchorage with a long post and the option for planning a "patient-specific bone graft" were also selected. The baseplate was positioned such that during preparation, the glenoid reamer would ream bone to the central post but not beyond (Fig. 1). Translation of the baseplate was performed to ensure that the baseplate was not seated on a peripheral glenoid rim osteophyte. To ensure the central post was centered in the deepest portion of the glenoid vault, the glenoid baseplate was positioned centrally in the inferior circle of the glenoid in an "en face" view. To limit variability among the 3 assessors and instead capture variability in patient anatomy, the angle of the glenoid reaming pin was positioned at zero degrees for both glenoid version and inclination.

Each plan resulted in a 2-dimensional (2D) image of the region of contact created by the reamer on the glenoid fossa and a corresponding 3D representation of the glenoid bone defect along with the patient-specific bone graft placed under a standard glenoid implant (Fig. 2). The maximum glenoid defect was then denoted on the 3D images by placing a red mark at the periphery of the patient-specific bone graft during the planning process using an oblique image ("Max. Defect" in Fig. 2 and Fig. 3). The digital ruler tool was also used to measure the maximum glenoid defect.

On the 2D images, mathematical principles were used to determine the exact center of the circle. Two chords across the circle were drawn, and the midpoint of each chord was marked. Lines were drawn from these midpoints extending in a perpendicular direction toward the center of the circle. The intersection of these lines marked the center of the circle. An approximate line-of-best-fit representing the point of contact between the glenoid reamer and bone was then estimated. This was performed using the high point on each side of the glenoid (ie, "Ream Line' in Fig. 2). The location of a point perpendicular to this best-fit line was then identified, using a perpendicular line which also passed through the center of the circle (ie, "Perpendicular" line in Fig. 2). The angle between this point, the center of the circle, and the 12 o'clock position on the glenoid was measured (Θ_2D in Fig. 2).

On the 3D images, the user's view was then rotated from an oblique view back to an "en face" view of the glenoid. Visualization of the red digital marker was ensured. An angle was then measured between the previously placed digital red marker (the location of the maximum bone defect), the center of the glenoid baseplate, and the 12 o'clock position on the baseplate (Θ_3D in Fig. 2). Duplicate sets of thirty 2D and thirty 3D images were obtained, giving a total of 120 images for the initial analysis by each of the 3 reviewers. Each reviewer measured the 2D images first and after one week had elapsed, measured the 3D images. The images were sorted into a random sequence using a random number generator so that they were not analyzed in the same order. To allow an assessment of intrarater reliability, this process was then repeated a second time using the identical images. This provided a total of 360 individual angles measured in the study.

Statistical analysis

Descriptive statistics were calculated. Two-dimensional and 3D angles were compared using null hypothesis significance testing, with a significance level of $\alpha = 0.05$. The correlation between the angles calculated from 2D and 3D images was assessed using Pearson's correlation coefficient. Intraclass correlation (ICC) was

Table II
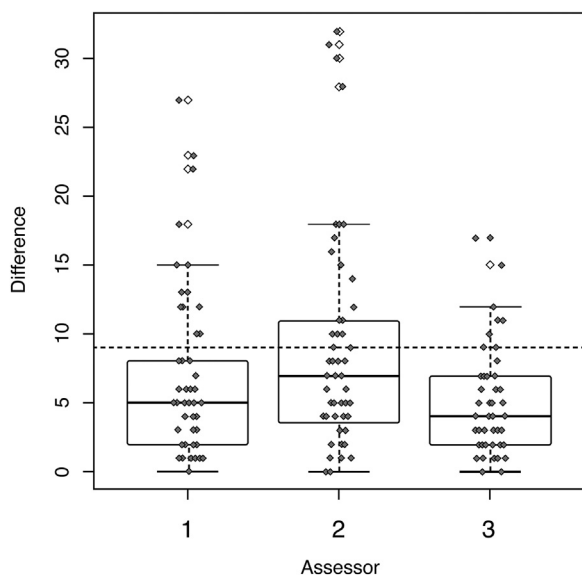Mean differences between 2D and 3D angle measurements.

Assessor	N	Difference in mean (SD)	Lower bound 95% CI	Upper bound 95% CI	P value
1	56	5.3 (5.1)	3.9	6.7	<.001
2	56	6.4 (6.1)	4.7	8.0	<.001
3	56	4.5 (4.1)	3.4	5.6	<.001
Total	168	5.4 (5.2)	4.6	6.2	<.001

2D, 2-dimensional; *3D*, 3-dimensional; *CI*, confidence interval; *SD*, standard deviation.
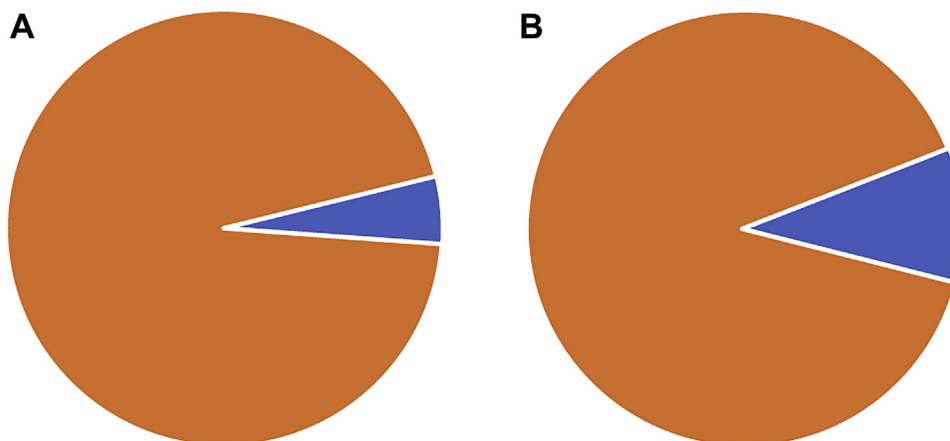
Figure 4 Visual representation of 5% (**A**) and 10% (**B**) circular arcs.

Figure 5 Absolute mean differences between 2D and 3D angles for each assessor. *2D*, 2-dimensional; *3D*, 3-dimensional.

used to assess interrater and intrarater reliability for both 2D and 3D angles. To assess precision, the proportion of defects lying within specific circular arcs was calculated. A 5% circular arc (or +/-9°) and a 10% circular arc (or +/-18°) were selected (Fig. 4). The proportion of patients for whom the maximal glenoid defect was found within these arcs was compared between reviewers using a Chi-square test.

Results

Of the 30 CT scans evaluated, one was excluded because of a previous open surgical procedure and one was excluded owing to technical limitations of the planning software resulting in an obscured view of the glenoid anatomy in both cases. Of the 28 included patients, 18 had a diagnosis of osteoarthritis with an average retroversion of 27° (range 10° to 44°). The remaining 10 patients had a diagnosis of cuff tear arthropathy with an average superior inclination of 14° (4° to 23°) (Table I). Three reviewers measured each of 28 2D images twice, resulting in 168 2D angles for the final analysis. The same number of 3D angles was included for the final statistical analysis. The overall mean difference identified between the 2D and 3D angle measurements was 5.4° (standard deviation 5.2°). No significant differences were identified between 2D and 3D angles for each assessor (P = .205-.329) and for all angles together (P = .366) (Table II). The absolute differences between 2D and 3D angles for each assessor are demonstrated in Figure 5. The correlation between 2D and 3D angles for each reviewer is demonstrated in Table III and was almost perfect (Pearson's correlation overall ρ = 0.990). In addition, ICC results demonstrated almost perfect agreement for interrater reliability (ICC > 0.98 between all raters for both 2D and 3D angles) and intrarater reliability (ICC > 0.99 for each rater) (Tables III and IV). The results of the precision analysis demonstrated that the maximum glenoid defect was within a 5% circular arc from perpendicular to the high-side ream best-fit line in 143 of 168 (85.1%) comparisons and within a 10% circular arc in 164 of 168 (97.6%) comparisons. When the proportion of cases with maximum defects located inside these circular arcs were compared between assessors, no significant differences were found (P = .359).

Discussion

Glenoid bone defects are frequently encountered in primary RSA,[12] and the surgical management of these defects presents an

Table III
The correlation between 2D and 3D angle measurements and intrarater reliability.

Assessor	N	Pearson's ρ	ICC	95% CI
1	56	0.990	1.00	0.99-1.00
2	56	0.987	1.00	0.99-1.00
3	56	0.991	1.00	0.99-1.00
Total	168	0.990	1.00	0.99-1.00

2D, 2-dimensional; *3D*, 3-dimensional; *CI*, confidence interval; *ICC*, intraclass correlation.

Table IV
Interrater reliability for 2D and 3D angle measurements.

Angle measured	ICC (all assessors)	Lower bound 95% CI	Upper bound 95% CI
θ_2D	0.986	0.978	0.991
θ_3D	0.985	0.977	0.991

2D, 2-dimensional; *3D*, 3-dimensional; *CI*, confidence interval; *ICC*, intraclass correlation.

ongoing technical challenge.[20,23,24] Bone grafting is an important and biologically favorable method to address glenoid bone defects,[1,3,4,6,13,14,18] with high rates of graft incorporation reported in the literature.[16] The goal of the present study was to identify the location of the maximal depth of the glenoid bone defect in a variety of glenoid deformities. The key finding in our study is that the absolute mean difference between 2D and 3D angles measured was approximately 5.4° (with SD = 5.2°). The interpretation of this result is that the maximum glenoid deformity is located approximately perpendicular to the glenoid ream line to within an error of 5°. To our knowledge, this is a novel result, representing the first time the maximal glenoid defect has been localized using this method of landmarking. In addition, this novel method of glenoid defect localization does not depend on the underlying glenoid classification or etiology, broadening its applicability. To further expand these results, if our specific preoperative planning methodology was followed, the results could theoretically be applied clinically in the setting of either bone grafting or metal wedge augmentation, as a reference for graft or augment positioning.

When examined in combination, the results of this study suggest that they are statistically robust. The combination of small mean differences, very strong statistical correlation (>98%), and nearly perfect intrarater and interrater reliability (>98%) demonstrates that our results are very unlikely to be owing to chance alone. Given that a total of 168 pairwise comparisons were analyzed and given that the standard deviation of the underlying population of differences appears to be low, our study was adequately powered to detect statistical differences between 2D and 3D angle measurements.

Our results are further supported by the variability of glenoid defects included. A wide range of glenoid defects are encountered clinically,[9] and in this study, we were able to capture a substantial breadth of glenoid deformity as shown in Table I. The application of an agreed-upon and standardized preoperative planning procedure also contributed to a reduction in the overall sources of measurement errors in this study. Unfortunately, this also represents a limitation of our study. Given that the components used in planning, angle of glenoid reaming, and depth of glenoid reaming were standardized, the applicability of our results to the broader range of shoulder arthroplasty cases in the clinical setting is limited. The planning procedure used in this study was considered clinically acceptable, although it is perhaps not exactly the way that individual surgeons would choose to plan their cases, limiting its generalizability. This variability could lead to a change in the relative location of the maximum defect. Future work will focus on how alterations in guide pin placement alter the relative location of the

maximum glenoid defect. Other limitations of our study include the use of printed images for angle measurement (ie, nondigital). Digital image processing techniques may provide more precision in angular measurements.

The literature to date contains several described methods for the measurement of glenoid morphologic parameters such as glenoid version,[7,8,11,17,19] inclination,[2,21] and bone loss.[10,22] The methods used to date have been based on both plain radiographs and high-resolution CT scans. In addition, 3D CT-based preoperative planning software has been recently validated clinically and allows accurate characterization of glenoid morphology.[20] The maximum depth of the horizontal plane bone defect has been previously reported, although the methodology used applies only to Walch type B2 glenoids.[22] To our knowledge, no prior study has documented the association between the orientation of the glenoid ream line and the location of the maximum glenoid bone defect.

Conclusions

Using 3D CT-based planning software, we have demonstrated with almost perfect agreement among 3 assessors that the maximum glenoid bone defect is reliably and precisely located perpendicular to the glenoid ream line when the reaming axis is held constant. The results of this study may improve the preoperative planning process when reconstructing complex glenoid deformities with bone graft. Future directions include a second phase of the current protocol whereby surgeons will be permitted to position the glenoid baseplate in the desired location to best address the glenoid pathology identified to replicate the real (ie, intraoperative) environment, followed by a collection of similar data on the location of the maximal glenoid defect. Other future work may include the application of digital image processing techniques and the development of novel instrumentation for the preparation of patient-specific bone grafts during reverse shoulder arthroplasty.

Disclaimers:

References

1. Athwal GS, MacDermid JC, Reddy KM, Marsh JP, Faber KJ, Drosdowech D. Does bony increased-offset reverse shoulder arthroplasty decrease scapular notching? J Shoulder Elbow Surg 2015;24:468-73. https://doi.org/10.1016/j.jse.2014.08.015.

2. Boileau P, Cheval D, Gauci MO, Holzer N, Chaoui J, Walch G. Automated three-dimensional measurement of glenoid version and inclination in arthritic shoulders. J Bone Joint Surg Am 2018;100:57-65. https://doi.org/10.2106/JBJS.16.01122.

3. Boileau P, Morin-Salvo N, Bessière C, Chelli M, Gauci MO, Lemmex DB. Bony increased-offset-reverse shoulder arthroplasty: 5 to 10 years' follow-up. J Shoulder Elbow Surg 2020. https://doi.org/10.1016/j.jse.2020.02.008.

4. Boileau P, Morin-Salvo N, Gauci MO, Seeto BL, Chalmers PN, Holzer N, et al. Angled BIO-RSA (bony-increased offset-reverse shoulder arthroplasty): a solution for the management of glenoid bone loss and erosion. J Shoulder Elbow Surg 2017;26:2133-42. https://doi.org/10.1016/j.jse.2017.05.024.

5. Chae J, Siljander M, Wiater JM. Instability in reverse total shoulder arthroplasty. J Am Acad Orthop Surg 2018;26:587-96. https://doi.org/10.5435/JAAOS-D-16-00408.

6. Collin P, Liu X, Denard PJ, Gain S, Nowak A, Lädermann A. Standard versus bony increased-offset reverse shoulder arthroplasty: a retrospective comparative cohort study. J Shoulder Elbow Surg 2018;27:59-64. https://doi.org/10.1016/j.jse.2017.07.020.

7. Cunningham G, Freebody J, Smith MM, Taha ME, Young AA, Cass B, et al. Comparative analysis of 2 glenoid version measurement methods in variable axial slices on 3-dimensionally reconstructed computed tomography scans. J Shoulder Elbow Surg 2018;27:1809-15. https://doi.org/10.1016/j.jse.2018.03.016.

8. Ditzler MG, Kan JH, Artunduaga M, Jadhav SP, Bell BR, Zhang W, et al. Modified friedman technique: a new proposed method of measuring glenoid version in the setting of glenohumeral dysplasia. Pediatr Radiol 2018;48:1779-85. https://doi.org/10.1007/s00247-018-4196-7.

9. Frankle MA, Teramoto A, Luo ZP, Levy JC, Pupello D. Glenoid morphology in reverse shoulder arthroplasty: classification and surgical implications. J Shoulder Elbow Surg 2009;18:874-85. https://doi.org/10.1016/j.jse.2009.02.013.

10. Hill JM, Norris TR. Long-term results of total shoulder arthroplasty following bone-grafting of the glenoid. J Bone Joint Surg Am 2001;83:877-83.

11. Javed S, Hadi S, Imam MA, Gerogiannis D, Foden P, Monga P. The ellipse modification of the friedman method for measuring glenoid version. Bone Joint J 2020;102-B:232-8. https://doi.org/10.1302/0301-620X.102B2.BJJ-2019-0726.R1.

12. Klein SM, Dunning P, Mulieri P, Pupello D, Downes K, Frankle MA. Effects of acquired glenoid bone defects on surgical technique and clinical outcomes in reverse shoulder arthroplasty. J bone Joint Surg Am volume 2010;92:1144-54. https://doi.org/10.2106/JBJS.I.00778.

13. Klika BJ, Wooten CW, Sperling JW, Steinmann SP, Schleck CD, Harmsen WS, et al. Structural bone grafting for glenoid deficiency in primary total shoulder arthroplasty. J Shoulder Elbow Surg 2014;23:1066-72. https://doi.org/10.1016/j.jse.2013.09.017.

14. Lopiz Y, García-Fernández C, Arriaza A, Rizo B, Marcelo H, Marco F. Midterm outcomes of bone grafting in glenoid defects treated with reverse shoulder arthroplasty. J Shoulder Elbow Surg 2017;26:1581-8. https://doi.org/10.1016/j.jse.2017.01.017.

15. Mizuno N, Denard PJ, Raiss P, Walch G. Reverse total shoulder arthroplasty for primary glenohumeral osteoarthritis in patients with a biconcave glenoid. J Bone Joint Surg Am 2013;95:1297-304. https://doi.org/10.2106/JBJS.L.00820.

16. Paul RA, Maldonado-Rodriguez N, Docter S, Khan M, Veillette C, Verma N, et al. Glenoid bone grafting in primary reverse total shoulder arthroplasty: a systematic review. J Shoulder Elbow Surg 2019;28:2447-56. https://doi.org/10.1016/j.jse.2019.05.011.

17. Poon PC, Ting FS. A 2-dimensional glenoid vault method for measuring glenoid version on computed tomography. J Shoulder Elbow Surg 2012;21:329-35. https://doi.org/10.1016/j.jse.2011.04.006.

18. Riboh JC, Garrigues GE. Bone grafting in shoulder arthroplasty. Orthopedics 2012;35:966-73. https://doi.org/10.3928/01477447-20121023-11.

19. Rouleau DM, Kidder JF, Pons-Villanueva J, Dynamidis S, Defranco M, Walch G. Glenoid version: how to measure it? validity of different methods in two-dimensional computed tomography scans. J Shoulder Elbow Surg 2010;19:1230-7. https://doi.org/10.1016/j.jse.2010.01.027.

20. Seidl AJ, Williams GR, Boileau P. Challenges in reverse shoulder arthroplasty: Addressing glenoid bone loss. Orthopedics 2016;39:14-23. https://doi.org/10.3928/01477447-20160111-01.

21. Shukla DR, McLaughlin RJ, Lee J, Nguyen NTV, Sanchez-Sotelo J. Automated three-dimensional measurements of version, inclination, and subluxation. Shoulder Elbow 2020;12:31-7. https://doi.org/10.1177/1758573218825480.

22. Walch G, Moraga C, Young A, Castellanos-Rosas J. Results of anatomic non-constrained prosthesis in primary osteoarthritis with biconcave glenoid. J Shoulder Elbow Surg 2012;21:1526-33. https://doi.org/10.1016/j.jse.2011.11.030.

23. Werner BS, Böhm D, Abdelkawi A, Gohlke F. Glenoid bone grafting in reverse shoulder arthroplasty for long-standing anterior shoulder dislocation. J Shoulder Elbow Surg 2014;23:1655-61. https://doi.org/10.1016/j.jse.2014.02.017.

24. Werner BS, Hudek R, Burkhart KJ, Gohlke F. The influence of three-dimensional planning on decision-making in total shoulder arthroplasty. J Shoulder Elbow Surg 2017;26:1477-83. https://doi.org/10.1016/j.jse.2017.01.006.